Inorganic Chemistry

pubs.acs.org/IC

Article

Coordination Polymers from Biphenyl-Dicarboxylate Linkers: Synthesis, Structural Diversity, Interpenetration, and Catalytic Properties

Xiaoyan Cheng, Lirong Guo,* Hongyu Wang, Jinzhong Gu,* Ying Yang, Marina V. Kirillova, and Alexander M. Kirillov*

Cite This: *Inorg. Chem.* 2022, 61, 12577−12590

Read Online

ACCESS | Metrics & More | Article Recommendations | Supporting Information

ABSTRACT: The present work explores two biphenyl-dicarboxylate linkers, 3,3′-dihydroxy-(1,1′-biphenyl)-4,4′-dicarboxylic (H_4L_1) and 4,4′-dihydroxy-(1,1′-biphenyl)-3,3′-dicarboxylic (H_4L_2) acids, in hydrothermal generation of nine new compounds formulated as $[Co_2(\mu_2\text{-}H_2L_1)_2(phen)_2(H_2O)_4]$ (**1**), $[Mn_2(\mu_4\text{-}H_2L_1)_2(phen)_2]_n{\cdot}4nH_2O$ (**2**), $[Zn(\mu_2\text{-}H_2L_1)(2,2'\text{-bipy})(H_2O)]_n$ (**3**), $[Cd(\mu_2\text{-}H_2L_1)(2,2'\text{-bipy})(H_2O)]_n$ (**4**), $[Mn_2(\mu_2\text{-}H_2L_1)(\mu_4\text{-}H_2L_1)(\mu_2\text{-}4,4'\text{-bipy})_2]_n{\cdot}4nH_2O$ (**5**), $[Zn(\mu_2\text{-}H_2L_1)(\mu_2\text{-}4,4'\text{-bipy})]_n$ (**6**), $[Zn(\mu_2\text{-}H_2L_2)(phen)]_n$ (**7**), $[Cd(\mu_3\text{-}H_2L_2)(phen)]_n$ (**8**), and $[Cu(\mu_2\text{-}H_2L_2)(\mu_2\text{-}4,4'\text{-bipy})(H_2O)]_n$ (**9**). These coordination polymers (CPs) were generated by reacting a metal(II) chloride, a H_4L_1 or H_4L_2 linker, and a crystallization mediator such as 2,2′-bipy (2,2′-bipyridine), 4,4′-bipy (4,4′-bipyridine), or phen (1,10-phenanthroline). The structural types of **1**−**9** range from molecular dimers (**1**) to one-dimensional (**3**, **4**, **7**) and two-dimensional (**8**, **9**) CPs as well as three-dimensional metal−organic frameworks (**2**, **5**, **6**). Their structural, topological, and interpenetration features were underlined, including an identification of unique two- and fivefold 3D + 3D interpenetrated nets in **5** and **6**. Phase purity, thermal and luminescence behavior, as well as catalytic activity of the synthesized products were investigated. Particularly, a Zn(II)-based CP **3** acts as an effective and recyclable heterogeneous catalyst for Henry reaction between a model substrate (4-nitrobenzaldehyde) and nitroethane to give *β*-nitro alcohol products. For this reaction, various parameters were optimized, followed by the investigation of the substrate scope. By reporting nine new compounds and their structural traits and functional properties, the present work further outspreads a family of CPs constructed from the biphenyl-dicarboxylate H_4L_1 and H_4L_2 linkers.

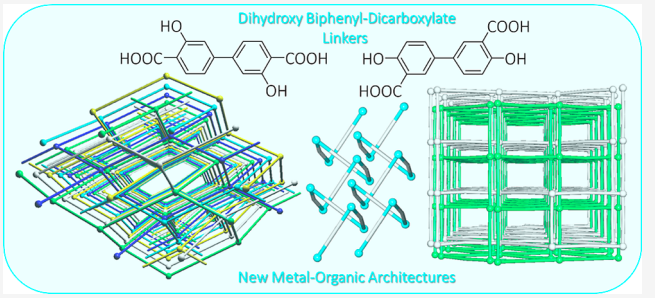

INTRODUCTION

Coordination polymers (CPs) and their porous subclass, well-known as MOFs (metal−organic frameworks), are currently of massive attention among researchers in areas of chemistry, physics, and material science.[1−6] Such a tremendous recognition of these metal−organic architectures is largely governed by their infinite diversity of structural types and enthralling functional properties and applications in a multitude of research areas, including storage and separation of gases,[7−13] sensing, luminescent and biomaterials,[14−19] and catalysis,[20−26] just to name a few.

Among a large variety of factors that may influence the assembly of CPs/MOFs,[27,28] the selection of a principal building block acting as a linker and its intrinsic characteristics represent a central parameter.[29,30] In addition, synthetic methods and reaction conditions can affect structural features and properties of the resulting compounds.[31−39] In this regard, hydrothermal synthesis stands out as one of the most promising and useful methodologies, owing to a blend of intrinsic pressure and temperature parameters for crystallizing the products and using H_2O as a green reaction medium.[40−43]

Multicarboxylic acids with aromatic cores possess great thermal stability and are the key building blocks for assembling CPs via hydrothermal synthesis.[29,44] An attractive use of these types of organic linkers in the field of CPs/MOFs is attributed to their rich coordination chemistry, different pK_a values, aqueous solubility in the form of reactive salt derivatives, and attractive physicochemical characteristics.[20,21,31,33,34,39,45,46]

As an exploration of recent research of our groups in the field of hydrothermal preparation of novel metal−organic architectures from multicarboxylate linkers, we devoted our attention to hydroxy functionalized biphenyl-dicarboxylate building blocks, namely, 3,3′-dihydroxy-(1,1′-biphenyl)-4,4′-dicarboxylic (H_4L_1) and 4,4′-dihydroxy-(1,1′-biphenyl)-3,3′-

Received: April 30, 2022
Published: August 3, 2022

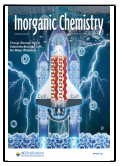

https://doi.org/10.1021/acs.inorgchem.2c01488
Inorg. Chem. 2022, 61, 12577−12590

dicarboxylic (H_4L_2) acids (Scheme 1).[47−52] The selection of these carboxylic acids was governed by the following points:

Scheme 1. Formulae of H_4L_1 and H_4L_2 Linkers and *N*-Donor Crystallization Mediators

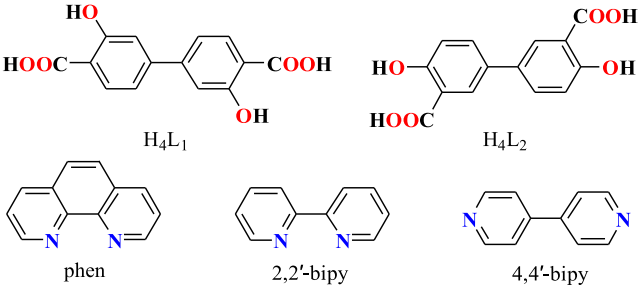

(i) both H_4L_1 and H_4L_2 are positional isomers with different locations of two COOH and two OH groups, (ii) the presence of biphenyl functionality permits some rotation along the carbon−carbon single bond, and (iii) both linkers are stable under hydrothermal conditions and can assume numerous modes of coordination. Given the extraordinary structural features and applications of some CPs/MOFs assembled from these types of ligands,[53−64] the main aim of the current study consisted in further exploring H_4L_1 and H_4L_2 as promising dicarboxylate linkers for generating new types of CPs, followed by the investigation of their structural traits and some functional properties.

Thus, the present study describes the preparation procedures, structural characterization, topology and interpenetration features, luminescence properties, thermal stability, and catalytic behavior (Henry reaction) of new metal−organic architectures prepared from H_4L_1 or H_4L_2 and supporting ligands that mediate the crystallization (Scheme 1). The generated compounds have the following formulae: $[Co_2(\mu_2\text{-}H_2L_1)_2(phen)_2(H_2O)_4]$ (**1**), $[Mn_2(\mu_4\text{-}H_2L_1)_2(phen)_2]_n{\cdot}4nH_2O$ (**2**), $[Zn(\mu_2\text{-}H_2L_1)(2,2'\text{-bipy})(H_2O)]_n$ (**3**), $[Cd(\mu_2\text{-}H_2L_1)(2,2'\text{-bipy})(H_2O)]_n$ (**4**), $[Mn_2(\mu_2\text{-}H_2L_1)(\mu_4\text{-}H_2L_1)(\mu_2\text{-}4,4'\text{-bipy})_2]_n{\cdot}4nH_2O$ (**5**), $[Zn(\mu_2\text{-}H_2L_1)(\mu_2\text{-}4,4'\text{-bipy})]_n$ (**6**), $[Zn(\mu_2\text{-}H_2L_2)(phen)]_n$ (**7**), $[Cd(\mu_3\text{-}H_2L_2)(phen)]_n$ (**8**), and $[Cu(\mu_2\text{-}H_2L_2)(\mu_2\text{-}4,4'\text{-bipy})(H_2O)]_n$ (**9**). These metal−organic architectures further broaden to new types of growing family of functional CPs generated from the biphenyl-dicarboxylate H_4L_1or H_4L_2 linkers.

EXPERIMENTAL SECTION

Brief Details on Synthesis of 1−9. Commercially acquired reagents and solvents were used (AR grade). All compounds (**1−9**) were synthesized hydrothermally using different compositions of the reaction mixtures in water, which are summarized in Table 1. These mixtures were treated for 72 h at 160 °C, followed by steady cooling for product crystallization with a rate of 10 °C h^{-1}. Detailed analytical data and synthesis procedures for each compound are given in the Supporting Information.

X-ray Diffraction. For single crystals of **1−9**, the X-ray data were obtained on a Bruker Smart CCD or an Agilent SuperNova diffractometer (graphite-monochromated Mo K_α radiation, λ = 0.71073 Å). Semiempirical absorption correction was performed with SADABS, whereas SHELXS-97/SHELXL-97[65,66] was applied for solving (direct methods) and refining (full-matrix least-squares on F^2) the structures. The non-hydrogen atoms were refined anisotropically (full-matrix least-squares on F^2), while the carbon-bound hydrogens were added to calculated positions with fixed isotropic thermal parameters. In COOH/H_2O moieties, hydrogen atoms were placed using difference maps and constrained to the respective parent oxygen atoms. In **2** and **5**, some very disordered solvent molecules were eliminated by applying SQUEEZE in PLATON.[67] The amount of crystallization molecules of solvent was calculated based on C/H/N and TGA analyses. In **4**, the OH group of $H_2L_1^{2-}$ was split over two sites and refined with 0.60 and 0.40 occupancies. In **5**, the OH moiety of $H_2L_1^{2-}$ was also split over two sites and refined with occupancies of 0.384 and 0.616. In **6**, the disordered aromatic ring of $H_2L_1^{2-}$ was refined with equal occupancies. A summary of crystal data for all the structures is provided in Table 2. Representative bonding parameters (Table S1) and hydrogen bond data (Table S2) are given in the Supporting Information.

In the obtained crystal structures, metal−organic (**2−9**) or H-bonded (**1**) networks were analyzed topologically by following a concept of underlying (simplified) network.[68,69] To obtain simplified metal−organic or H-bonded networks, the bridging ligands or molecular units were contracted, respectively, to the centroids while maintaining their connectivities.[55,56] CCDC2096490−2096498 enclose the crystallographic parameters of **1−9**.

Henry Reaction. Under typical conditions, a reaction mixture contained in a capped glass vessel and composed of 4-nitrobenzaldehyde (0.50 mmol; model substrate), nitroethane (2.0 mmol), and catalyst (4 mol %) in methanol (1.0 mL) was stirred for 12 h at 70 °C. The catalyst was then isolated through centrifuging the reaction mixture. The obtained solution was subjected to evaporation in vacuo to form a crude product. Its part was dissolved in deuterated chloroform for subsequent analysis by ^1H NMR spectroscopy using a JNM ECS 400 M spectrometer (for details, see Figure S4, Supporting Information). To carry out the catalyst recycling tests, after each reaction step, the catalyst was centrifuged, washed by methanol, desiccated, and used in the next cycle.

Table 1. Description of Hydrothermal Reaction Mixtures along with a Summary of Structural Features for Compounds 1−9[a]

compound	metal chloride precursor	supporting ligand as a mediator of crystallization (MC)	dimensionality	topology
$[Co_2(\mu_2\text{-}H_2L_1)_2(phen)_2(H_2O)_4]$ (**1**)	$CoCl_2{\cdot}6H_2O$	phen	0D	
$[Mn_2(\mu_4\text{-}H_2L_1)_2(phen)_2]_n{\cdot}4nH_2O$ (**2**)	$MnCl_2{\cdot}4H_2O$	phen	3D	**pts**
$[Zn(\mu_2\text{-}H_2L_1)(2,2'\text{-bipy})(H_2O)]_n$ (**3**)	$ZnCl_2$	2,2′-bipy	1D	2C1
$[Cd(\mu_2\text{-}H_2L_1)(2,2'\text{-bipy})(H_2O)]_n$ (**4**)	$CdCl_2{\cdot}H_2O$	2,2′-bipy	1D	2C1
$[Mn_2(\mu_2\text{-}H_2L_1)(\mu_4\text{-}H_2L_1)(\mu_2\text{-}4,4'\text{-bipy})_2]_n{\cdot}4nH_2O$ (**5**)	$MnCl_2{\cdot}4H_2O$	4,4′-bipy	3D + 3D[b]	**sqc65**
$[Zn(\mu_2\text{-}H_2L_1)(\mu_2\text{-}4,4'\text{-bipy})]_n$ (**6**)	$ZnCl_2$	4,4′-bipy	3D + 3D[c]	**dia**
$[Zn(\mu_2\text{-}H_2L_2)(phen)]_n$ (**7**)	$ZnCl_2$	phen	1D	2C1
$[Cd(\mu_3\text{-}H_2L_2)(phen)]_n$ (**8**)	$CdCl_2{\cdot}H_2O$	phen	2D	**utp**
$[Cu(\mu_2\text{-}H_2L_2)(\mu_2\text{-}4,4'\text{-bipy})(H_2O)]_n$ (**9**)	$CuCl_2{\cdot}2H_2O$	4,4′-bipy	2D	**hcb**

[a]Reactions were carried out under hydrothermal settings: stainless steel autoclave (25 mL volume with teflon lining), H_2O (10 mL), M^{2+}/H_4L/MC/NaOH molar ratio (1:1:1:2), 160 °C, 72 h. [b]Twofold interpenetrated nets. [c]Fivefold interpenetrated nets.

https://doi.org/10.1021/acs.inorgchem.2c01488
Inorg. Chem. 2022, 61, 12577−12590

Table 2. Crystallographic Data for Compounds 1−9

compound	1	2	3	4	5
chemical formula	$C_{26}H_{20}CoN_2O_8$	$C_{52}H_{40}Mn_2N_4O_{16}$	$C_{24}H_{18}ZnN_2O_7$	$C_{24}H_{18}CdN_2O_7$	$C_{24}H_{19}MnN_2O_8$
formula weight	547.37	1086.69	511.77	558.80	518.32
crystal system	Triclinic	triclinic	monoclinic	orthorhombic	monoclinic
space group	$P\bar{1}$	$P\bar{1}$	$I2/a$	$Pcab$	$P1_2/c1$
a/Å	7.51048(13)	14.04807(16)	18.4131(2)	6.93160(10)	14.4043(4)
b/Å	10.16251(14)	14.08253(15)	7.82310(10)	23.5275(3)	11.6030(3)
c/Å	15.9746(2)	14.09923(17)	30.0763(4)	28.1740(3)	17.3938(5)
α/°	101.6072(12)	61.7498(12)	90	90	90
β/°	101.8231(13)	79.7349(11)	96.0530(10)	90	107.851(3)
γ/°	99.9253(13)	73.1773(10)	90	90	90
V/Å^3	1139.62(3)	2349.09(5)	4308.26(9)	4594.71(10)	2767.12(14)
T/K	293(2)	293(2)	293(2)	293(2)	293(2)
Z	2	2	8	8	4
D_c/g cm^{-3}	1.595	1.435	1.578	1.616	1.158
μ/mm^{-1}	6.411	4.958	2.030	8.034	4.183
F(000)	562	1036	2096	2240	984
refl. measured	14270	35015	14701	15495	16555
unique refl. (R_{int})	4211 (0.0338)	8689 (0.0486)	3993 (0.0251)	4160 (0.0294)	5345 (0.0920)
GOF on F^2	1.044	1.008	1.087	1.042	1.107
R_1 [$I > 2\sigma(I)$]	0.0315	0.0403	0.0371	0.0288	0.0844
wR_2 [$I > 2\sigma(I)$]	0.0804	0.1021	0.1090	0.0807	0.1039

compound	6	7	8	9
chemical formula	$C_{24}H_{16}ZnN_2O_6$	$C_{26}H_{16}ZnN_2O_6$	$C_{26}H_{16}CdN_2O_6$	$C_{24}H_{17}CuN_2O_7$
formula weight	493.76	517.78	564.81	508.93
crystal system	triclinic	orthorhombic	orthorhombic	triclinic
space group	$P\bar{1}$	$Pna2_1$	$Pna2_1$	$P\bar{1}$
a/Å	8.86840(10)	13.0069(4)	10.1025(4)	8.6127(6)
b/Å	11.0591(2)	15.7790(5)	10.2188(4)	9.3670(6)
c/Å	11.96730(10)	10.7000(4)	20.7971(8)	13.4134(6)
α/°	85.4940(10)	90	90	99.604(5)
β/°	76.8250(10)	90	90	94.884(5)
γ/°	71.8150(10)	90	90	99.304(6)
V/Å^3	1085.70(3)	2196.01(13)	2147.00(15)	1045.91(11)
T/K	293(2)	293(2)	293(2)	293(2)
Z	2	4	4	2
D_c/g cm^{-3}	1.510	1.566	1.747	1.616
μ/mm^{-1}	1.958	1.969	8.573	1.934
F(000)	504	1056	1128	520
refl. measured	10798	8426	2755	6468
unique refl. (R_{int})	4249 (0.0376)	3044 (0.0417)	2328 (0.0398)	3324 (0.0431)
GOF on F^2	1.172	1.079	1.045	1.053
R_1 [$I > 2\sigma(I)$]	0.0686	0.0350	0.0351	0.0716
wR_2 [$I > 2\sigma(I)$]	0.0709	0.0411	0.0477	0.1095

Successive reaction cycles were accomplished as mentioned above. Various blank tests were run to confirm the importance of coordination compounds as catalysts. Effects of various reaction conditions such as temperature, time, solvent, and substrate scope were also investigated.

RESULTS AND DISCUSSION

Hydrothermal Synthesis of 1−9. Both carboxylic acid building blocks, 3,3′-dihydroxy-(1,1′-biphenyl)-4,4′-dicarboxylic acid (H_4L_1) and 4,4′-dihydroxy-(1,1′-biphenyl)-3,3′-dicarboxylic acid (H_4L_2), represent up to six potential O-sites for coordination. To further explore their application toward the design of novel CPs/MOFs, several hydrothermal reactions were attempted using aqueous mixtures composed of M(II) chlorides [M(II) = Co, Mn, Zn, Cd, Cu], H_4L_1 or H_4L_2 as a linker, NaOH as a base, and a series of crystallization mediators (Scheme 1). These auxiliary ligands were 2,2′-bipy(2,2′-bipyridine), 4,4′-bipy(4,4′-bipyridine), or phen(1,10-phenanthroline), Among various reactions attempted, nine hydrothermal syntheses were well reproducible and permitted an isolation of pure crystalline product fractions (Table 1) that also contained monocrystals appropriate for X-ray diffraction study. In contrast to H_4L_1, the products derived from H_4L_2 turned to be more difficult to crystallize, and we were able to isolate only three compounds (**7**−**9**). The manganese(II) CP **2** and MOF **5** reveal different structural types owing to different crystallization mediators (phen for **2** or 4,4′-bipy for **5**); in the latter case, the μ_2-4,4′-bipy acts as an additional linker that is responsible for increasing the dimensionality to a 3D net. Similarly, the structures of Zn(II) CPs **3** and **6** are also affected by the type of crystallization mediator, revealing 1D chains or 3D frameworks, respectively. CPs **5** and **6** were synthesized using the same procedure but altering the metal(II) precursor

https://doi.org/10.1021/acs.inorgchem.2c01488
Inorg. Chem. 2022, 61, 12577−12590

Scheme 2. Coordination Modes for $H_2L_1^{2-}$ (Modes I–IV) and $H_2L_2^{2-}$ (Modes V–VII) in Structures of 1–9

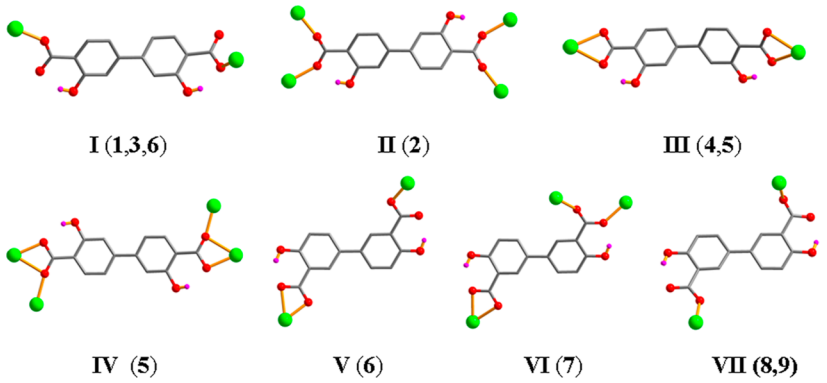

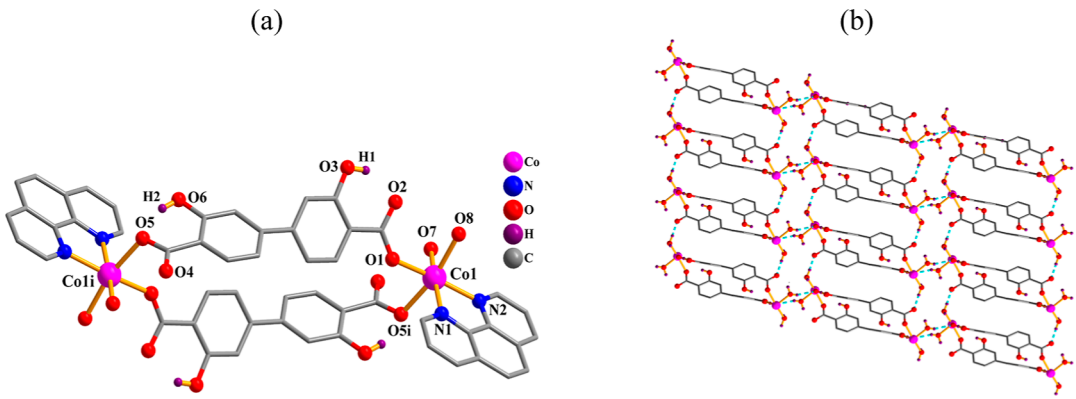

Figure 1. Crystal structure of compound **1**. (a) Co_2 dimer; only OH hydrogen atoms are shown; (b) 2D H-bonded layer; phen ligands are not shown; representation along the *b*-axis.

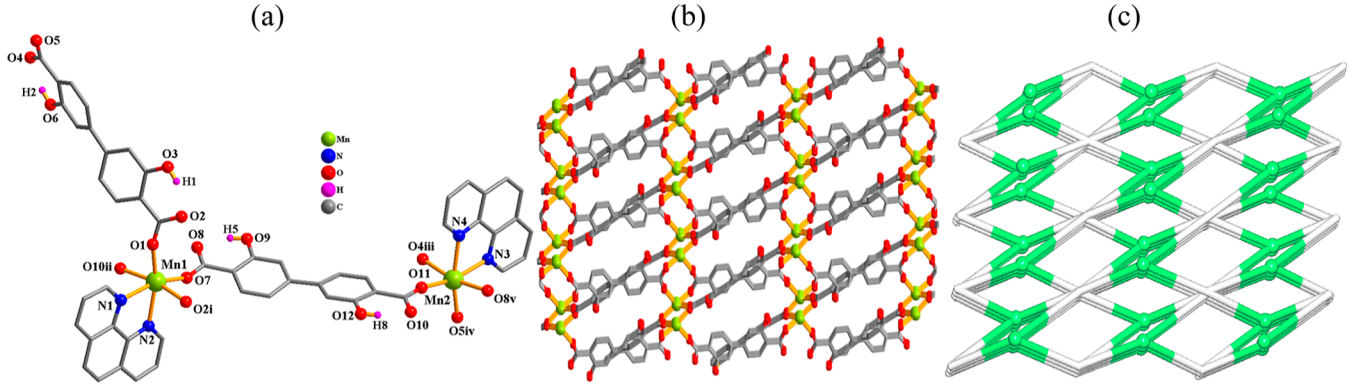

Figure 2. Crystal structure of **2**. (a) Connectivity and coordination environments of metal atoms; CH atoms are not shown. (b) 3D MOF; phen ligands are omitted; view along the *a*-axis. (c) Topological view of a dinodal 4,4-connected **pts** network; representation along the *a*-axis; centroids of 4-linked μ_4-$H_2L_1^{2-}$ nodes (gray); 4-linked Mn nodes (green balls).

($MnCl_2$ for **5** and $ZnCl_2$ for **6**), resulting in 3D interpenetrated nets in both cases but with different topologies and degrees of interpenetration. The structures of **7** and **8** are also affected by the type of metal precursor used, despite the similarity of other reaction conditions. With regard to the type of biphenyl-dicarboxylate linker, the direct comparison of the isolated products is difficult as not all synthetic attempts resulted in the isolation of pure crystalline products. For example, when using the same crystallization mediator (phen), the products derived from H_4L_1 were isolated in the case of Co(II) and Mn(II), while similar reactions with H_4L_2 permitted to crystallize only zinc(II) and cadmium(II) derivatives (Table 1). Nevertheless, zinc(II) derivatives **3** and **7** with closely related supporting ligands (2,2′-bipy and phen) feature similar types of 1D CP structures. In contrast, the Cd(II) products **4** (1D CP) and **8** (2D CP) show a difference in their dimensionality and topology that is likely influenced by the type of biphenyl–dicarboxylate linker.

In general, structural differences in **1**–**9** indicate that their metal–organic architectures depend on crystallization mediator, metal precursor, and main dicarboxylic acid linker (with COOH and OH groups in different positions of the biphenyl core). The biphenyl–dicarboxylate linkers exhibit up to seven distinct coordination modes (Scheme 2) with COO^- groups of different denticities. Also, the $H_2L_1^{2-}/H_2L_2^{2-}$ linkers in **1**–**9** feature a rotation of the rings along the C–C bond with the

https://doi.org/10.1021/acs.inorgchem.2c01488
Inorg. Chem. 2022, 61, 12577–12590

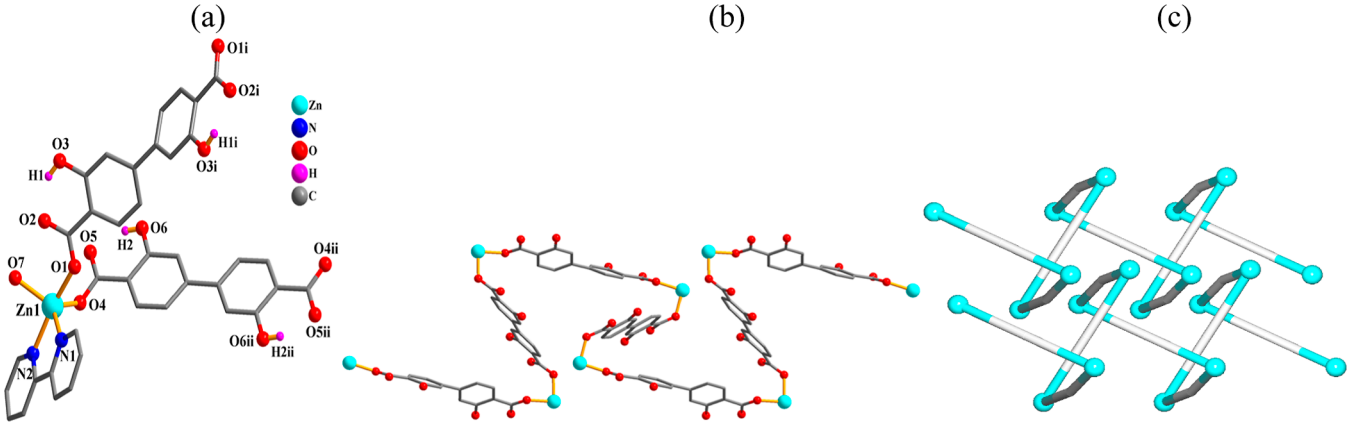

Figure 3. Crystal structure of **3**. (a) Connectivity and coordination environment of metal center; CH atoms are not shown. (b) Helical metal−organic chain; 2,2′-bipy ligands are omitted; representation along the *c*-axis. (c) Topological view of two helical 2C1 chains; centroids of μ_2-$H_2L_1^{2-}$ linkers (gray); Zn atoms (turquoise balls).

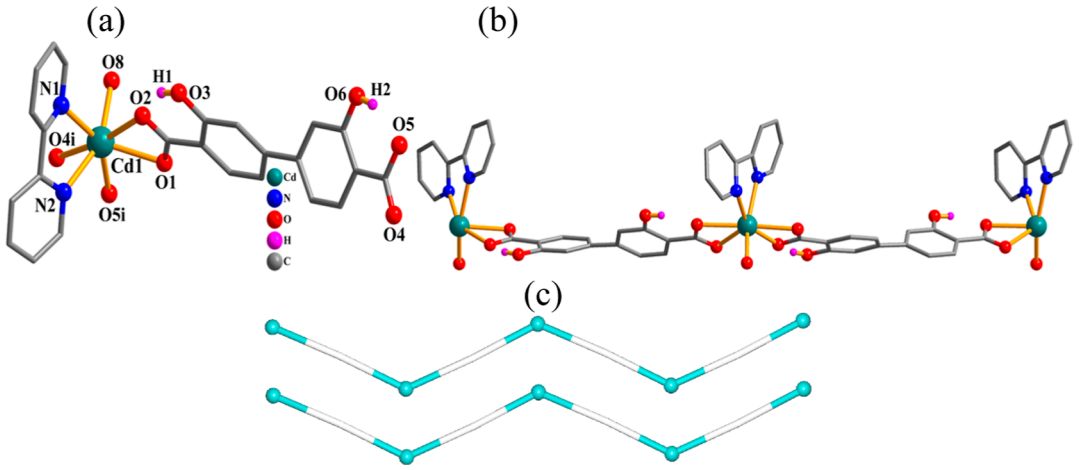

Figure 4. Crystal structure of **4**. (a) Connectivity and coordination environment of metal center; CH atoms are not shown. (b) 1D CP chain; representation along the *a*-axis. (c) Topological view of two 2C1 chains; centroids of μ_2-$H_2L_1^{2-}$ linkers (gray), Cd atoms (turquoise balls).

corresponding angles (dihedral) ranging from 0.0 to 46.21°, thus enabling an adjustment of ligands to coordination preferences of metal ions. All new compounds were fully characterized in the solid state, including the determination of crystal structures by X-ray diffraction (Table 2). The latter disclose molecular dimers (**1**), one-dimensional (**3**, **4**, **7**) and two-dimensional (**8**, **9**) CPs as well as three-dimensional (**2**, **5**, **6**) metal−organic networks.

Structural Description. *$[Co_2(\mu_2\text{-}H_2L_1)_2(phen)_2(H_2O)_4]$ (**1**).* The structure of **1** reveals a dimeric complex (Figure 1) that contains one Co(II) atom, one μ_2-$H_2L_1^{2-}$ linker, one phen ligand, and two terminal water ligands in the asymmetric entity. Both six-coordinate Co1 centers display a distorted $\{CoN_2O_4\}$ octahedral environment that is constructed from two carboxylate oxygen atoms from two μ_2-$H_2L_1^{2-}$ blocks, a pair of N_{phen} atoms, and two water ligands. The distances of Co−N [2.123(2)−2.132(2) Å] and Co−O [2.042(2)−2.184(2) Å] bonds agree with typical literature data.[21,31,70] Two $H_2L_1^{2-}$ ligands act as μ_2-linkers via monodentate carboxylate groups (Scheme 2, mode I), thus assembling two Co1 centers to give a cyclic Co_2 complex with a Co···Co separation of 14.056(2) Å (Figure 1a). Such Co_2 molecular units are involved in an intermolecular H-bonding forming a 2D network (Figure 1b) with an **sql** topology.[71,72]

*$[Mn_2(\mu_4\text{-}H_2L_1)_2(phen)_2]_n \cdot 4nH_2O$ (**2**).* An asymmetric unit of this 3D MOF contains two manganese(II) atoms, two μ_4-$H_2L_1^{2-}$ ligands, and two terminal phen moieties (Figure 2). The Mn1/Mn2 centers are six-coordinate and assume the distorted octahedral $\{MnN_2O_4\}$ environments (Figure 2a). These are filled by four oxygen atoms from four μ_4-$H_2L_1^{2-}$ linkers and two N_{phen} donors. The distances of the Mn−N [2.301(2)−2.308(2) Å] and Mn−O [2.087(2)−2.209(2) Å] bonds are within typical values.[31,39,46] The $H_2L_1^{2-}$ ligands function as μ_4-linkers with carboxylate functionalities adopting μ_2-bridging bidentate modes (Scheme 2, mode II). These dicarboxylate linkers multiply sew the Mn(II) centers into a 3D MOF (Figure 2b). Topologically, MOF **2** is constructed from the 4-linked Mn(II) and μ_4-H_2L_1 nodes, forming a dinodal 4,4-linked framework of a **pts** [PtS, Cooperite] topological type with a $(4^2.8^4)$ point symbol (Figure 2c).[73]

*$[Zn(\mu_2\text{-}H_2L_1)(2,2'\text{-bipy})(H_2O)]_n$ (**3**).* This CP reveals a 1D helical chain structure (Figure 3) composed of a zinc(II) center, two-halves of μ_2-$H_2L_1^{2-}$ linker, a 2,2′-bipy ligand, and a terminal water ligand per asymmetric unit. The Zn1 atom is five-coordinate and shows a distorted trigonal bipyramidal $\{ZnN_2O_3\}$ environment (Figure 3a), which is taken by a pair of O donors from two μ_2-$H_2L_1^{2-}$ blocks, one water ligand, and a pair of $N_{2,2'\text{-bipy}}$ atoms. The lengths of Zn−N [2.095(2)−2.113(2) Å] and Zn−O [1.990(2)−2.041(2) Å] bonds are

https://doi.org/10.1021/acs.inorgchem.2c01488
Inorg. Chem. 2022, 61, 12577−12590

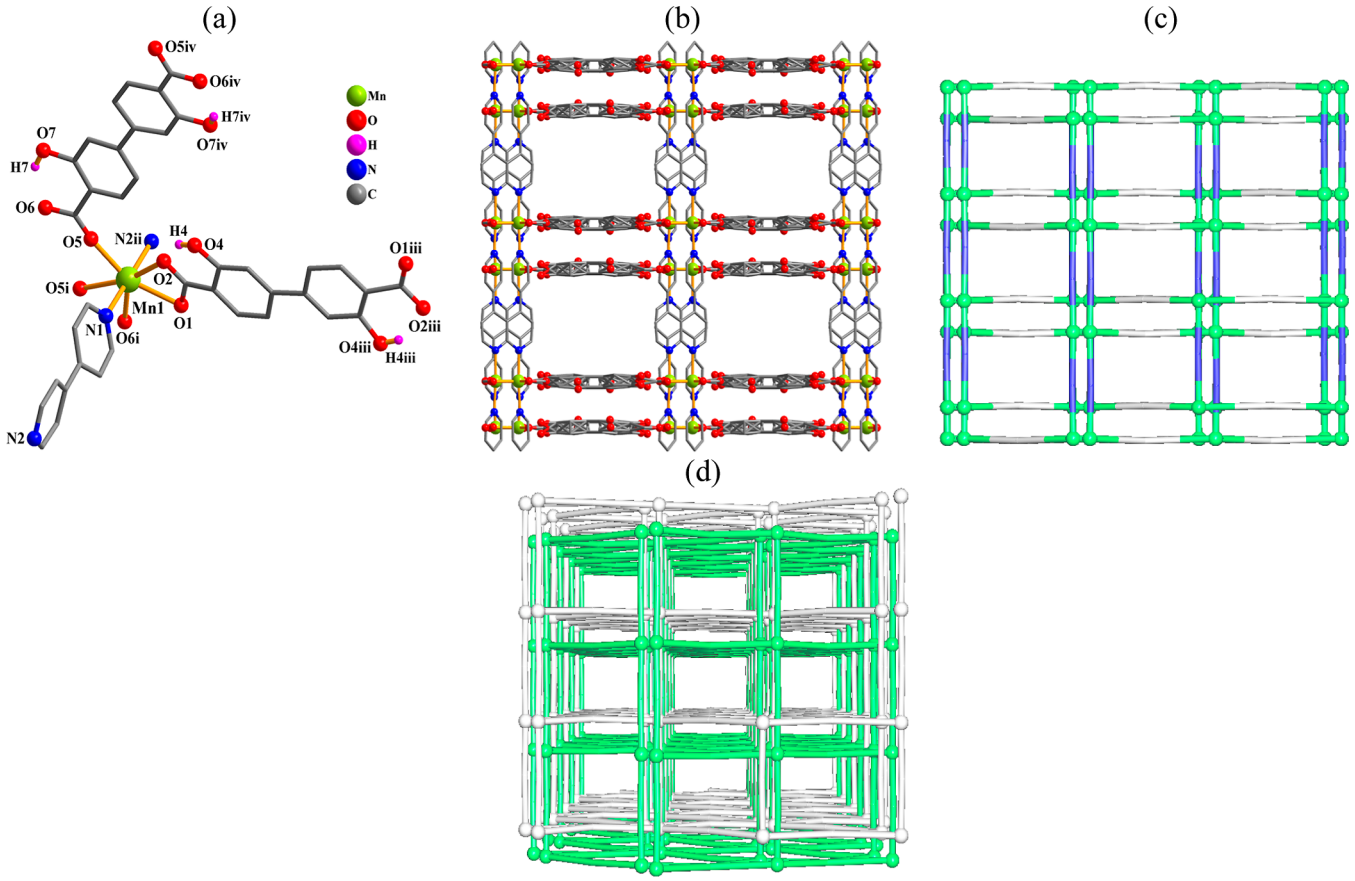

Figure 5. Crystal structure of **5**. (a) Connectivity and coordination environment metal atom; CH atoms are not shown. (b) Three-dimensional MOF; view along the *c*-axis. (c) Topological view of a dinodal 4,5-linked network with an **sqc65** topology; view along the *c*-axis; centroids of 2- and 4-linked μ_2- and μ_4-$H_2L_1^{2-}$ nodes (gray), centroids of 2-linked μ_2-4,4′-bipy moieties (blue), and 5-linked Mn nodes (green balls). (d) Perspective view of two interpenetrated frameworks represented by green and gray colors.

standard for such type of compounds.[31,74,75] The $H_2L_1^{2-}$ block behaves as a μ-linker (Scheme 2, mode I), bridging the Zn1 centers into one-dimensional helical chains (Figure 3b) with a Zn1···Zn1 separation of 15.495(3) Å. These chains feature a 2C1 topology (Figure 3c).

[Cd(μ_2-H_2L_1)(2,2′-bipy)(H_2O)]$_n$ ***(4)***. The one-dimensional CP **4** comprises a Cd1 atom, a μ_2-$H_2L_1^{2-}$ linker, a 2,2′-bipy moiety, and a water ligand per asymmetric unit (Figure 4). The Cd1 atom is seven-coordinate and possesses a distorted $\{CdN_2O_5\}$ pentagonal bipyramidal environment. It is constructed from four carboxylate oxygen donors from a pair of μ_2-$H_2L_1^{2-}$ linkers, two $N_{2,2'\text{-bipy}}$ atoms, and an H_2O ligand (Figure 4a). The $H_2L_1^{2-}$ ligand assumes a μ_2-coordination mode with bidentate carboxylate functionalities (Scheme 2, mode III). The $H_2L_1^{2-}$ linkers connect the Cd(II) atoms into 1D chains of a 2C1 topological type (Figure 4b,c).

[Mn_2(μ_2-H_2L_1)(μ_4-H_2L_1)(μ_2-4,4′-bipy)$_2$]$_n$·4nH_2O ***(5)***. This compound possesses a 3D MOF structure (Figure 5). It comprises a Mn1 atom, a half of μ_2-$H_2L_1^{2-}$ and a half of μ_4-$H_2L_1^{2-}$ linkers, a μ_2-4,4′-bipy moiety, and two crystallization water molecules in the asymmetric unit. The seven-coordinate Mn1 center reveals a distorted $\{MnN_2O_5\}$ pentagonal bipyramidal fashion. The coordination sphere contains five oxygen atoms from three $H_2L_1^{2-}$ linkers and two nitrogen atoms from two different 4,4′-bipy ligands (Figure 5a). The Mn−N [2.256(4)−2.259(4) Å] and Mn−O [2.212(3)−2.504(3) Å] distances well compare with typical values.[31,39,63] The $H_2L_1^{2-}$ blocks exhibit μ_2- or μ_4-coordination fashions with carboxylate moieties being bridging tridentate or bidentate (Scheme 2, modes IV and III). These dicarboxylate linkers, along with additional μ_2-4,4′-bipy pillars, connect the Mn1 atoms into a three-dimensional MOF (Figure 5c). Topologically, the structure is composed of the 5-connected Mn nodes, 2- and 4-linked μ_2- and μ_4-$H_2L_1^{2-}$ blocks, and 2-linked μ_2-4,4′-bipy moieties. A binodal 4,5-connected network is generated (Figure 5c) and can be classified within an **sqc65** (epinet) type. It has a $(4^2.6^4)$ $(4^3.6^7)_2$ point symbol with the $(4^2.6^4)$ and $(4^3.6^7)$ notations referring to the μ_4-$H_2L_1^{2-}$ and Mn nodes, respectively. A remarkable peculiarity of **5** also consists in two interpenetrated networks (Figure 5d) having the parameters as follows: class IIa; total degree of interpenetration, Z = 2; interpenetration primitive cell, PIC: [1,0,0][0,0,1][0,1,0].

[Zn(μ_2-H_2L_1)(μ_2-4,4′-bipy)]$_n$ ***(6)***. This compound also shows an interpenetrated 3D MOF structure (Figure 6). Its asymmetric unit holds a Zn1 center, two halves of μ_2-$H_2L_1^{2-}$ ligands, and two halves of μ_2-4,4′-bipy ligands. The four-coordinate Zn1 center unveils a trigonal pyramidal $\{ZnN_2O_2\}$ coordination fashion with two carboxylate oxygen donors from a pair of μ_2-$H_2L_1^{2-}$ ligands and two nitrogen donors from two μ_2-4,4′-bipy linkers (Figure 6a). The Zn−N [2.055(4)−2.059(5) Å] and Zn−O [1.922(4)−1.964(4) Å] bonds well agree with typical values for this type of compounds.[31,56,74] The $H_2L_1^{2-}$ ligands act as μ_2-linkers (Scheme 2, mode I) with monodentate carboxylate functionalities. The μ_2-$H_2L_1^{2-}$ and μ_2-4,4′-bipy ligands connect the Zn1 centers to produce a 3D MOF structure (Figure 6b). Topologically, the structure

https://doi.org/10.1021/acs.inorgchem.2c01488
Inorg. Chem. 2022, 61, 12577−12590

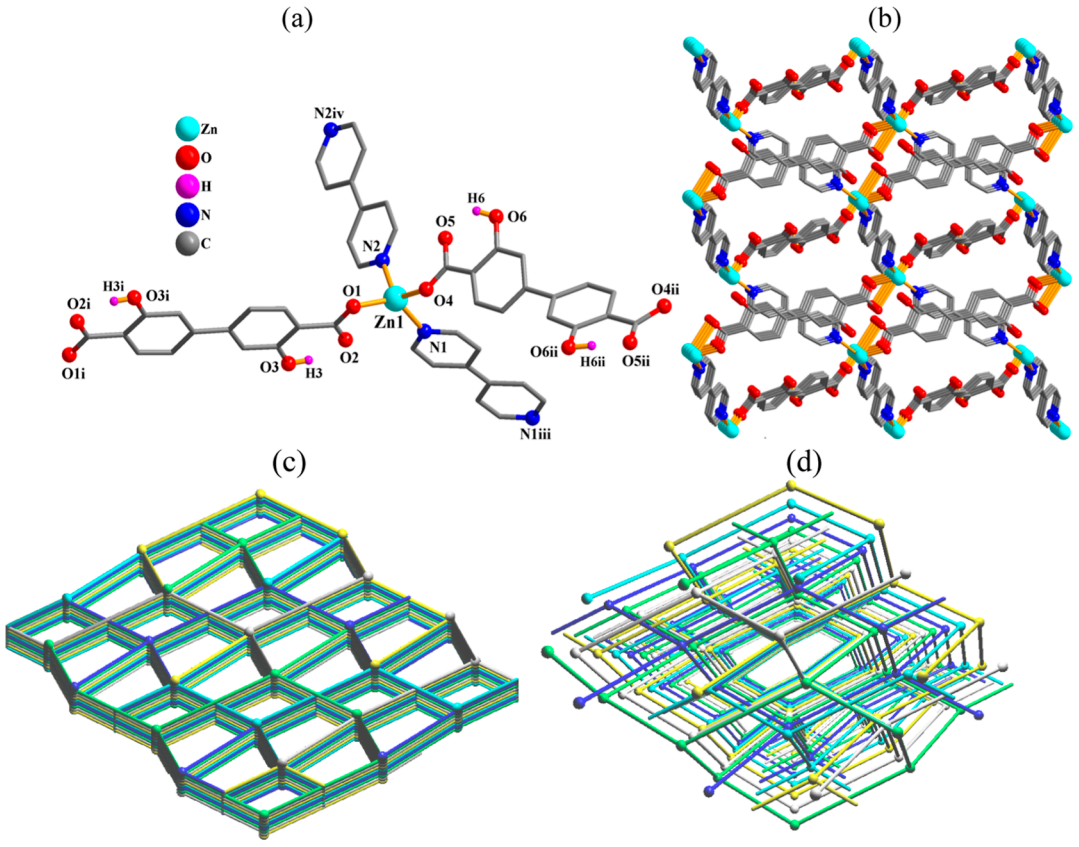

Figure 6. Crystal structure of **6**. (a) Connectivity and coordination environment of metal atom; CH atoms are not shown. (b) 3D MOF; view along the *a*-axis. (c) Topological view of a mononodal 4-linked **dia** network; representation along the *a*-axis; centroids of 2-linked μ_2-$H_2L_1^{2-}$ and μ_2-4,4′-bipy moieties (sticks), 4-linked Zn nodes (balls). (d) Perspective view of five interpenetrated frameworks represented in green, blue, cyan, yellow, and gray colors.

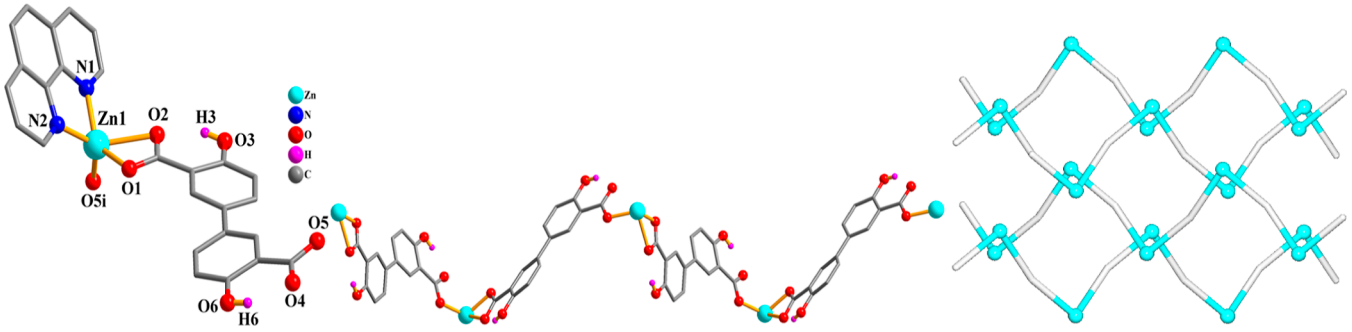

Figure 7. Crystal structure of **7**. (a) Connectivity and coordination environment of metal atom; CH atoms are not shown. (b) 1D zigzag chain; phen ligands are omitted; representation along the *c*-axis. (c) Topological view of four zigzag chains of the 2C1 type; centroids of μ_2-$H_2L_2^{2-}$ linkers (gray), Zn atoms (turquoise balls).

comprises the 4-linked Zn nodes and the 2-linked μ_2-$H_2L_1^{2-}$ and μ_2-4,4′-bipy moieties (Figure 6c), generating a uninodal 4-connected net of the **dia** topological type with a point symbol of (6^6). As in the case of **5**, compound **6** also features interpenetration, but remarkably, there are five 3D + 3D interpenetrated nets (Figure 6d) having the parameters as follows: class Ia; total degree of interpenetration, Z = 5; interpenetration primitive cell, PIC: [5,0,0][0,1,1][2,0,1].

[Zn(μ_2-H_2L_2)(phen)]$_n$ (**7**). This 1D CP (Figure 7) contains a Zn(II) atom, a μ_2-$H_2L_2^{2-}$ block, and a terminal phen ligand per asymmetric entity (Figure 7a). The five-coordinate Zn1 center assumes a distorted trigonal bipyramidal {ZnN_2O_3} geometry that is built from three carboxylate oxygen atoms from two μ_2-$H_2L_2^{2-}$ linkers and two N_{phen} atoms. The Zn−N [2.072(5)−2.078(5) Å] and Zn−O [1.939(3)−2.329(4) Å] bonding distances agree with related literature data.[31,56,75] The $H_2L_2^{2-}$ block functions as a μ_2-linker with mono- and bidentate carboxylate groups (Scheme 2, mode V). The carboxylate moieties are responsible for interconnection of Zn(II) atoms to produce 1D zigzag chains (Figure 7b) of a 2C1 topological type (Figure 7c).

[Cd(μ_3-H_2L_2)(phen)]$_n$ (**8**). This 2D CP (Figure 8) comprises a Mn(II) atom, a μ_3-$H_2L_2^{2-}$ linker, and a phenanthroline ligand in the asymmetric unit. The six-coordinate Cd1 center exhibits a distorted octahedral {CdN_2O_4} coordination environment, which is occupied by four oxygen donors from

https://doi.org/10.1021/acs.inorgchem.2c01488
Inorg. Chem. 2022, 61, 12577−12590

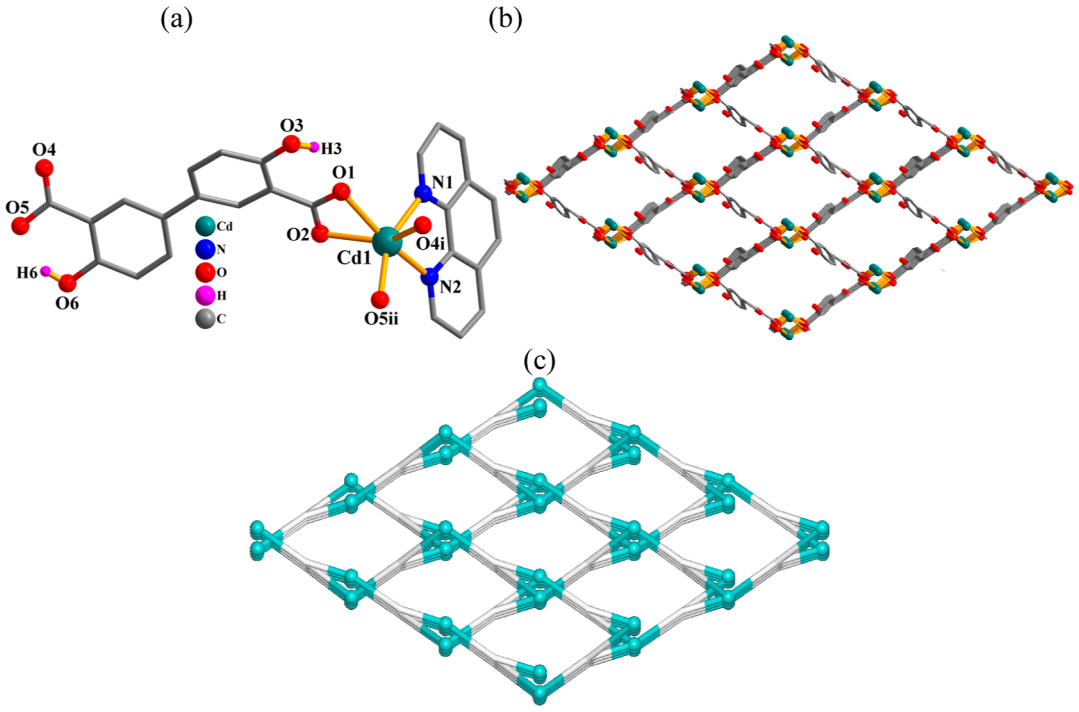

Figure 8. Crystal structure of **8**. (a) Connectivity and coordination environment of metal atom; CH atoms are not shown. (b) 2D metal−organic layer; phen ligands are omitted; representation along the *a*-axis. (c) Topological view of a uninodal 3-linked **utp** network; representation along the *a*-axis; centroids of 3-linked μ_2-$H_2L_2^{2-}$ nodes (gray), 3-linked Cd nodes (turquoise balls).

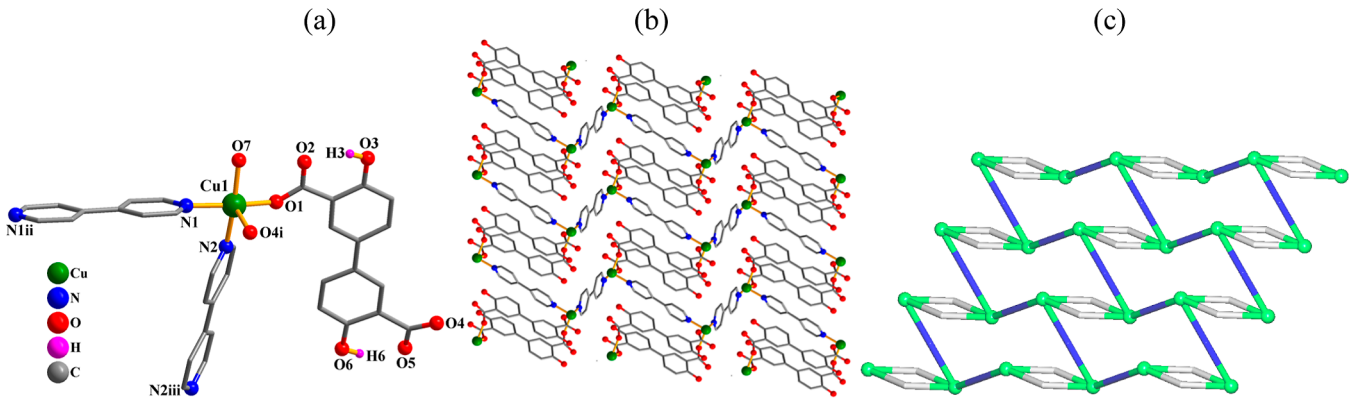

Figure 9. Crystal structure of **9**. (a) Connectivity and coordination environment of metal atom; CH atoms are not shown. (b) 2D CP layer; representation along the *ac* plane. (c) Topological representation of a mononodal 3-linked **hcb** net; representation along the *b*-axis; centroids of 2-connected μ_2-$H_2L_2^{2-}$ (gray) and μ_2-4,4′-bipy (blue) linkers, 3-linked Cu nodes (green balls).

three μ_3-$H_2L_2^{2-}$ ligands and two N_{phen} donors (Figure 8a). The bonding Cd−N [2.300(7)−2.368(7) Å] and Cd−O [2.220(6)−2.348(6) Å] distances reveal usual values.[31,39,76] The $H_2L_2^{2-}$ ligand functions as a μ_3-linker (Scheme 2, mode VI) with bridging bidentate and bidentate carboxylate functionalities. The Cd(II) centers are united via the μ_3-$H_2L_2^{2-}$ ligands to form a two-dimensional coordination network (Figure 8b). It is assembled from the 3-linked Cd and μ_3-$H_2L_2^{2-}$ nodes that are topologically similar and give rise to a mononodal 3-connected net of a **utp** topological type; point symbol is (10^3) (Figure 8c).[77,78]

[Cu(μ_2-H_2L_2)(μ_2-4,4′-bipy)(H_2O)]$_n$ (**9**). This CP also displays a 2D layer structure (Figure 9). The asymmetric entity encompasses a copper(II) atom, a μ_2-$H_2L_2^{2-}$ linker, a μ_2-4,4′-bipy linker, and a water ligand. The Cu1 center is five-coordinate and discloses a distorted trigonal bipyramidal {CuN_2O_3} environment. This is populated by a pair of oxygen atoms from two μ_2-$H_2L_2^{2-}$ ligands, one water ligand, and two nitrogen atoms from a pair of μ_2-4,4′-bipy linkers (Figure 9a). The Cu−N [2.000(3)−2.019(3) Å] and Cu−O [1.939(2)−2.184(3) Å] bonds agree with distances in related compounds.[20,75,79] The $H_2L_2^{2-}$ block acts as a μ-linker (Scheme 2, mode VII) with monodentate COO^- groups. The Cu(II) centers are held together via the μ_2-$H_2L_2^{2-}$ and μ_2-4,4′-bipy ligands into a 2D layer (Figure 9b). Topologically, it can be defined as a mononodal 3-linked net of a **hcb** [Shubnikov hexagonal plane net/(6,3)] type (Figure 9c).[74,79]

PXRD and TGA. For **1**−**9**, powder X-ray diffraction (PXRD) patterns were measured at ambient conditions (Figure S2, Supporting Information), revealing a good phase purity for all the compounds. This was established by

https://doi.org/10.1021/acs.inorgchem.2c01488
Inorg. Chem. 2022, 61, 12577−12590

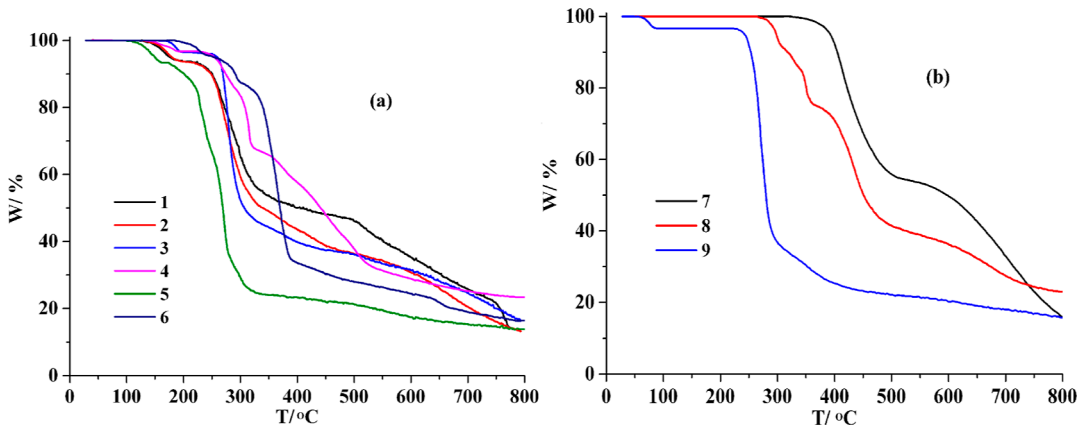

Figure 10. TGA traces for compounds **1**–**9** (25–800 °C, 10 °C/min, N_2 flow).

comparing experimental diffraction patterns with those calculated using CIF files.

Thermogravimetric analysis (TGA) was performed to study the thermal behavior of **1**–**9** under nitrogen flow (Figure 10). For **1**, a release of four H_2O ligands is seen in the 126–198 °C interval (exptl, 6.4%; calcd, 6.6%), and the decomposition starts at 208 °C. Compound **2** discloses an elimination of four crystallization H_2O molecules at 128–200 °C (exptl, 6.5%; calcd, 6.6%), pursued by degradation of the resulting solid starting from 218 °C. Compound **3** releases its water ligand between 167 and 199 °C (exptl, 3.6%; calcd, 3.5%) and the degradation of metal–organic network starts at 250 °C. Similarly, compound **4** reveals a thermal effect at 140–192 °C due to a loss of H_2O ligand (exptl, 3.3%; calcd, 3.2%), pursued by the start of the degradation at 228 °C. In the case of CP **5**, there is a loss of two lattice H_2O molecules (exptl, 6.7%; calcd, 6.9%) at 108–161 °C, prior to the decomposition at 174 °C. Compounds **6**–**8**, which do not contain H_2O ligands or solvent molecules, maintain stability up to 184, 330, and 263 °C, respectively. In the case of compound **9**, a loss of water ligand (exptl, 3.4%; calcd, 3.5%) is observed in the 58–87 °C range; the resulting sample is then stable up to 227 °C.

Catalytic Activity in Henry Reaction. The Henry reaction, also known as nitroaldol transformation, represents an important carbon–carbon bond-forming technique in organic synthesis, wherein nitroalkanes are combined with carbonyl substrates (aldehydes, ketones) to generate beta-nitro alcohol products. Generally, this type of reaction requires a base as a catalyst, such as alkoxide, alkali metal hydroxide, or amine.[80−84] Considering possible use of different CPs as heterogeneous catalytic systems in the Henry transformation that can proceed in the absence of base,[81−83] the catalytic behavior of **1**–**9** was explored in the transformations involving various aldehyde substrates and nitroethane to give the corresponding β-nitro alcohol products. As a model substrate, 4-nitrobenzaldehyde was chosen (Scheme 3 and Table 3) and the impact of various reaction conditions was monitored (e.g., reaction time, type of solvent, and amount of catalyst and its recycling).

Within the tested series of compounds **1**–**9**, the zinc(II) CP $[Zn(\mu_2\text{-}H_2L_1)(2,2'\text{-bipy})(H_2O)]_n$ (**3**) revealed the most promising catalytic activity (Table 3) and thus was investigated in more detail. In contrast to **3**, other tested compounds showed lower efficiency with total product yields between 25 and 66% (Table 3, entries 18–25).

Scheme 3. Henry Reaction of 4-Nitrobenzaldehyde (Model Substrate) with Nitroethane under Optimized Conditions

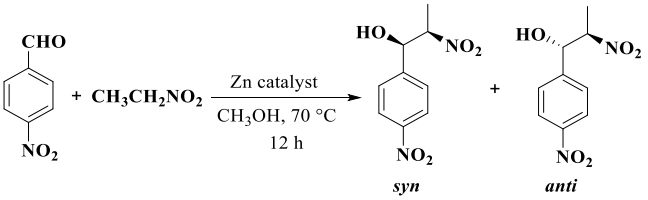

In the reaction catalyzed by **3**, there is an accumulation of two isomers of β-nitro alcohol products with a rise of the total yield from 36% to 90% when the reaction time was increased from 1 to 16 h (entries 1–7, Table 3; Figure S5, Supporting Information). However, the reaction is almost complete after 12 h (89% yield), and this time was used in further experiments. The catalyst amount also has an influence on the total yield, leading to its increase from 81% to 90% on varying the catalyst loading from 3 to 5 mol % (entries 7, 12, and 13). Although methanol appeared to be the solvent of choice, a number of additional solvents were screened, but these were less efficient. The following tendency in the total product yields was observed (Table 3, entries 7, 14–17): CH_3OH (89%) > H_2O (76%) > THF (66%) > C_2H_5OH (52%) > CH_3CN (10%). Although there is no clear connection between the activity and structure of the catalyst, a superior performance of compound **3** might be related to its 1D chain structure and/or existence of open Zn sites and labile water ligands.[75,79,83,84] Compound **3** with a 1D structure features a better accessibility of metal centers if compared to MOF **6** with a 3D structure. This likely explains superior catalytic performance of **3**.[81,82] Besides, we have to highlight that the present Henry reactions between 4-nitrobenzaldehyde and nitroethane do not occur in the catalyst's absence or applying organic H_4L_1 and H_4L_2 precursors as catalysts (no products were detected in all cases). Furthermore, the use of $ZnCl_2$ or 2,2′-bipy as a potential catalyst revealed only low product yields of 12% and 15%, respectively (Table 3, entries 26–30). An important observation also concerns the fact that in the reactions catalyzed by **3**, there is no formation of byproducts as attested by NMR analysis (Figure S4). With regard to selectivity to syn and anti product isomers, their formation in close to equal amounts is generally observed, as expected for such type of reactions that lead to diastereomeric mixtures.[80]

https://doi.org/10.1021/acs.inorgchem.2c01488
Inorg. Chem. 2022, 61, 12577−12590

Table 3. Catalysis Data in the Henry Reaction of 4-Nitrobenzaldehyde and Nitroethane[a]

entry	catalyst	time (h)	amount of catalyst (mol %)	temp. (°C)	Solvent	yield (%)[b]	selectivity[c] (syn/anti)
1	**3**	1	4	70	CH_3OH	36	56:44
2	**3**	2	4	70	CH_3OH	53	55:45
3	**3**	4	4	70	CH_3OH	63	56:44
4	**3**	6	4	70	CH_3OH	73	55:45
5	**3**	8	4	70	CH_3OH	83	55:45
6	**3**	10	4	70	CH_3OH	87	54:46
7	**3**	12	4	70	CH_3OH	89	55:45
8	**3**	16	4	70	CH_3OH	90	55:45
9	**3**	12	4	25	CH_3OH	16	56:44
10	**3**	12	4	60	CH_3OH	73	54:46
11	**3**	12	4	80	CH_3OH	88	54:46
12	**3**	12	3	70	CH_3OH	81	55:45
13	**3**	12	5	70	CH_3OH	90	55:45
14	**3**	12	4	70	H_2O	76	55:45
15	**3**	12	4	70	CH_3CN	10	40:60
16	**3**	12	4	70	THF	66	44:66
17	**3**	12	4	70	C_2H_5OH	52	54:46
18	**1**	12	4	70	CH_3OH	55	54:46
19	**2**	12	4	70	CH_3OH	54	55:45
20	**4**	12	4	70	CH_3OH	57	54:46
21	**5**	12	4	70	CH_3OH	25	56:44
22	**6**	12	4	70	CH_3OH	66	56:44
23	**7**	12	4	70	CH_3OH	36	55:45
24	**8**	12	4	70	CH_3OH	25	54:46
25	**9**	12	4	70	CH_3OH	41	44:45
26	no catalyst	12	–	70	CH_3OH	–	–
27	$ZnCl_2$	12	4	70	CH_3OH	12	43:57
28	2,2′-bipy	12	4	70	CH_3OH	15	58:42
29	H_4L_1	12	4	70	CH_3OH	–	–
30	H_4L_2	12	4	70	CH_3OH	–	–
31	$ZnCl_2$ + H_4L_1	12	4 + 4	70	CH_3OH	9	42:58
32	$ZnCl_2$ + H_4L_2	12	4 + 4	70	CH_3OH	8	40:60

[a]Typical reaction conditions (unless stated otherwise): aldehyde substrate (0.5 mmol), nitroethane (2.0 mmol), catalyst (4.0 mol.%), CH_3OH (1.0 mL), 12 h, 70 °C. [b]Total product yields were calculated from the ^1H NMR data: [moles of products per mol of substrate (aldehyde)] × 100%. [c]Molar ratio between syn and anti isomers of β-nitro alcohol products.

Using the optimized reaction conditions, we also explored catalyst **3** for studying the substrate scope on different aldehydes (Table 4). Substituted benzaldehydes, cinnamaldehyde, and acetaldehyde were tested in the Henry reaction, leading to total product yields in the 20−92% range. In comparison to benzaldehyde (81% product yield), substituted benzaldehydes containing an electron-withdrawing functionality (e.g., $-NO_2$, −Cl) revealed similar or increased product yields (81−90%; Table 4, entries 1−5); this can be potentially related to enhanced electrophilicity of these aldehydes. However, the aldehyde substrates bearing electron-donating functionalities (e.g., −OH, $-CH_3$, $-OCH_3$) and cinnamaldehyde displayed inferior yields of products (20−60%; Table 4, entries 6−9).

Table 4. Henry Reaction between Different Aldehydes and Nitroethane in the Presence of Catalyst **3**[a]

entry	benzaldehyde (RC_6H_4CHO) or other aldehyde substrate	product yield (%)[b]	selectivity (syn/anti)[c]
1	R = H	81	51:49
2	R = 2-NO_2	82	58:42
3	R = 3-NO_2	85	55:45
4	R = 4-NO_2	89	55:45
5	R = 4-Cl	81	50:50
6	R = 4-OH	60	56:44
7	R = 4-CH_3	56	43:57
8	R = 4-OCH_3	20	45:54
9	cinnamaldehyde	56	57:43
10	Acetaldehyde	92	56:44

[a]Reaction parameters: aldehyde substrate (0.5 mmol), nitroethane (2.0 mmol), CP **3** (4.0 mol %), CH_3OH (1.0 mL), 12 h, 70 °C. [b]Yields were calculated from the ^1H NMR data: [moles of products per mol of substrate (aldehyde)] × 100%. [c]Molar ratio between syn and anti isomers of β-nitro alcohol products.

The stability of catalyst **3** and its performance after recycling were also evaluated (conditions of Table 3, entry 7). The results of these catalytic experiments along with PXRD data (Figures S6 and S7, Supporting Information) point out that compound **3** preserves its structure and features, resembling catalytic performance during five reaction cycles. This can be evidenced by almost constant yields of products, a minor decline of which is likely associated with a minor loss of catalyst after several recycling experiments. In a model reaction involving 4-nitrobenzaldehyde and nitroethane as substrates, the catalytic performance of **3** is comparable to other heterogeneous catalytic systems based on metal-carboxylate coordination compounds (Table S3, Supporting Informa-

https://doi.org/10.1021/acs.inorgchem.2c01488
Inorg. Chem. 2022, 61, 12577−12590

tion)[81−86] or is superior if the reaction time is taken into consideration. Apart from high activity, good stability, and recyclability of **3**, this catalyst can lead to excellent product yields in a shorter reaction time.

For these Henry reactions, a possible mechanism was proposed on the basis of prior research studies describing related transformations that involve aldehydes and nitroethane and are catalyzed by CPs (Figure S8, Supporting Information).[87−89] Hence, there is an initial activation of both 4-nitrobenzaldehyde and nitroethane via an interaction with Zn(II) sites of the CP (Figure S8, step i). Such an interaction augments electrophilicity of 4-nitrobenzaldehyde and acidity of nitroethane. Subsequently, a reactive nitronate species is produced via deprotonation of the activated acidic nitroethane (step ii). Then, the new C−C bond is formed by nucleophilic attack of nitronate ion to coordinated 4-nitrobenzaldehyde (step iii). Finally, the next molecule of 4-nitrobenzaldehyde binds to the zinc(II) center, resulting in the release of the corresponding β-nitro alcohol product and completion of the catalytic cycle (Figure S8, step iv).

CONCLUSIONS

In the present work, the use of 3,3′-dihydroxy-(1,1′-biphenyl)-4,4′-dicarboxylic (H_4L_1) and 4,4′-dihydroxy-(1,1′-biphenyl)-3,3′-dicarboxylic (H_4L_2) acids was further explored in the hydrothermal generation of nine new coordination compounds **1**−**9**. All the obtained products were completely characterized, and their structures and topologies were established. Remarkably, crystal structures of MOFs **5** and **6** disclosed two- or fivefold 3D + 3D interpenetrated nets, respectively, thus contributing to broadening an important family of interpenetrated metal−organic architectures.[90,91]

Apart from standard investigation of thermal stability and luminescence characteristics, the obtained products were screened as catalysts in the Henry reaction between aldehydes and nitroethane to give β-nitro alcohol products. A zinc(II) 1D CP **3** revealed a particularly notable catalytic behavior that was optimized to a variety of reaction parameters and substrate scope, thus leading to up to 90% total product yields. Furthermore, this catalyst exhibited good stability and the possibility of reuse for five cycles.

In summary, the obtained compounds represent novel examples of metal−organic architectures that were hydrothermally assembled from hydroxy-functionalized biphenyl dicarboxylate blocks and different types of crystallization mediators. These results will stimulate further use of H_4L_1, H_4L_2 and related dicarboxylate linkers for generating functional CPs and MOFs.

ASSOCIATED CONTENT

Supporting Information

The Supporting Information is available free of charge at https://pubs.acs.org/doi/10.1021/acs.inorgchem.2c01488.

Full synthetic procedures and analytical data for **1**−**9**, FTIR spectra, PXRD patterns, luminescence data, catalysis data, and bonding parameters (PDF)

Accession Codes

CCDC 2096490−2096498 contain the supplementary crystallographic data for this paper. These data can be obtained free of charge via www.ccdc.cam.ac.uk/data_request/cif, or by emailing data_request@ccdc.cam.ac.uk, or by contacting The Cambridge Crystallographic Data Centre, 12 Union Road, Cambridge CB2 1EZ, UK; fax: +44 1223 336033.

AUTHOR INFORMATION

Corresponding Authors

Lirong Guo − *State Key Laboratory of Applied Organic Chemistry, Key Laboratory of Nonferrous Metal Chemistry and Resources Utilization of Gansu Province, College of Chemistry and Chemical Engineering, Lanzhou University, Lanzhou 730000, People's Republic of China*; Email: guolr@lzu.edu.cn

Jinzhong Gu − *State Key Laboratory of Applied Organic Chemistry, Key Laboratory of Nonferrous Metal Chemistry and Resources Utilization of Gansu Province, College of Chemistry and Chemical Engineering, Lanzhou University, Lanzhou 730000, People's Republic of China*; orcid.org/0000-0001-6704-7370; Phone: +86-931-8915196; Email: gujzh@lzu.edu.cn

Alexander M. Kirillov − *Centro de Química Estrutural, Institute of Molecular Sciences, Departamento de Engenharia Química, Instituto Superior Técnico, Universidade de Lisboa, Lisbon 1049-001, Portugal*; orcid.org/0000-0002-2052-5280; Phone: +351-218419396; Email: kirillov@tecnico.ulisboa.pt

Authors

Xiaoyan Cheng − *State Key Laboratory of Applied Organic Chemistry, Key Laboratory of Nonferrous Metal Chemistry and Resources Utilization of Gansu Province, College of Chemistry and Chemical Engineering, Lanzhou University, Lanzhou 730000, People's Republic of China*

Hongyu Wang − *State Key Laboratory of Applied Organic Chemistry, Key Laboratory of Nonferrous Metal Chemistry and Resources Utilization of Gansu Province, College of Chemistry and Chemical Engineering, Lanzhou University, Lanzhou 730000, People's Republic of China*

Ying Yang − *State Key Laboratory of Applied Organic Chemistry, Key Laboratory of Nonferrous Metal Chemistry and Resources Utilization of Gansu Province, College of Chemistry and Chemical Engineering, Lanzhou University, Lanzhou 730000, People's Republic of China*; orcid.org/0000-0002-6441-4064

Marina V. Kirillova − *Centro de Química Estrutural, Institute of Molecular Sciences, Departamento de Engenharia Química, Instituto Superior Técnico, Universidade de Lisboa, Lisbon 1049-001, Portugal*

Complete contact information is available at: https://pubs.acs.org/10.1021/acs.inorgchem.2c01488

Author Contributions

The manuscript was written through contributions of all authors.

Notes

The authors declare no competing financial interest.

ACKNOWLEDGMENTS

This work was supported by the 111 Project of MOE (111-2-17); the Major Science and Technology Projects by Gansu Province, China (19ZD2GC001); the Foundation for Science and Technology (FCT) and Portugal 2020 (projects CEECIND/03708/2017, PTDC/QUI-QIN/3898/2020, LIS-

BOA-01-0145-FEDER-029697, UIDB/00100/2020, and LA/P/0056/2020).

REFERENCES

(1) Batten, S. R.; Neville, S. M.; Turner, D. R. *Coordination Polymers: Design, Analysis and Application*; RSC Publication, 2009.
(2) *The Chemistry of Metal-Organic Frameworks: Synthesis, Characterization, and Applications*; Kaskel, S., Ed.; John Wiley & Sons, 2016.
(3) Öhrström, L.; Amombo Noa, F. M. *Metal-Organic Frameworks*; American Chemical Society, 2021.
(4) Morris, R. E.; Brammer, L. Coordination change, lability and hemilability in metal-organic frameworks. *Chem. Soc. Rev.* **2017**, *46*, 5444−5462.
(5) Chakraborty, G.; Park, I.-H.; Medishetty, R.; Vittal, J. J. Two-Dimensional Metal-Organic Framework Materials: Synthesis, Structures, Properties and Applications. *Chem. Rev.* **2021**, *121*, 3751−3891.
(6) Tabacaru, A.; Pettinari, C.; Galli, S. Coordination polymers and metal-organic frameworks built up with poly(tetrazolate) ligands. *Coord. Chem. Rev.* **2018**, *372*, 1−30.
(7) Cai, G.; Yan, P.; Zhang, L.; Zhou, H.-C.; Jiang, H.-L. Metal-Organic Framework-Based Hierarchically Porous Materials: Synthesis and Applications. *Chem. Rev.* **2021**, *121*, 12278−12326.
(8) McHugh, L. N.; Terracina, A.; Wheatley, P. S.; Buscarino, G.; Smith, M. W.; Morris, R. E. Metal-Organic Framework-Activated Carbon Composite Materials for the Removal of Ammonia from Contaminated Airstreams. *Angew. Chem., Int. Ed.* **2019**, *58*, 11747−11751.
(9) Lee, J. H.; Jeoung, S.; Chung, Y. G.; Moon, H. R. Elucidation of flexible metal-organic frameworks: Research progresses and recent developments. *Coord. Chem. Rev.* **2019**, *389*, 161−188.
(10) *Gas Adsorption in Metal-Organic Frameworks: Fundamentals and Applications*; Grant Glover, T., Mu, B., Eds.; CRC Press, 2018.
(11) Gu, C.; Hosono, N.; Zheng, J.-J.; Sato, Y.; Kusaka, S.; Sakaki, S.; Kitagawa, S. Design and control of gas diffusion process in a nanoporous soft crystal. *Science* **2019**, *363*, 387.
(12) Verdegaal, W. M.; Wang, K.; Sculley, J. P.; Wriedt, M.; Zhou, H.-C. Evaluation of Metal-Organic Frameworks and Porous Polymer Networks for CO_2-Capture Applications. *ChemSusChem* **2016**, *9*, 636−643.
(13) Li, H.; Wang, K.; Feng, D.; Chen, Y.-P.; Verdegaal, W.; Zhou, H.-C. Incorporation of Alkylamine into Metal-Organic Frameworks through a Bronsted Acid-Base Reaction for CO_2 Capture. *Chemsuschem* **2016**, *9*, 2832−2840.
(14) Cui, Y.; Yue, Y.; Qian, G.; Chen, B. Luminescent Functional Metal-Organic Frameworks. *Chem. Rev.* **2012**, *112*, 1126−1162.
(15) Kaur, H.; Sundriyal, S.; Pachauri, V.; Ingebrandt, S.; Kim, K.-H.; Sharma, A. L.; Deep, A. Luminescent metal-organic frameworks and their composites: Potential future materials for organic light emitting displays. *Coord. Chem. Rev.* **2019**, *401*, 213077.
(16) Vasylevskyi, S. I.; Bassani, D. M.; Fromm, K. M. Anion-Induced Structural Diversity of Zn and Cd Coordination Polymers Based on Bis-9,10-(pyridine-4-yl)-anthracene, Their Luminescent Properties, and Highly Efficient Sensing of Nitro Derivatives and Herbicides. *Inorg. Chem.* **2019**, *58*, 5646−5653.
(17) Fernandes, T. A.; Costa, I. F. M.; Jorge, P.; Sousa, A. C.; André, V.; Cerca, N.; Kirillov, A. M. Silver(I) Coordination Polymers Immobilized into Biopolymer Films for Antimicrobial Applications. *ACS Appl. Mater. Interfaces* **2021**, *13*, 12836−12844.
(18) Tibbetts, I.; Kostakis, G. E. Recent bio-advances in metal-organic frameworks. *Molecules* **2020**, *25*, 1291.
(19) Wang, C.; Wang, W.; Tan, J.; Zhang, X.; Yuan, D.; Zhou, H.-C. Coordination-based molecular nanomaterials for biomedically relevant applications. *Coord. Chem. Rev.* **2021**, *438*, 213752.
(20) Gu, J. Z.; Wen, M.; Cai, Y.; Shi, Z.; Arol, A. S.; Kirillova, M. V.; Kirillov, A. M. Metal-Organic Architectures Assembled from Multifunctional Polycarboxylates: Hydrothermal Self-Assembly, Structures, and Catalytic Activity in Alkane Oxidation. *Inorg. Chem.* **2019**, *58*, 2403−2412.
(21) Antonangelo, A. R.; Bezzu, C. G.; McKeown, N. B.; Nakagaki, S. Highly active manganese porphyrin-based microporous network polymers for selective oxidation reactions. *J. Catal.* **2019**, *369*, 133−142.
(22) Dong, L.; Chen, F.-E. Asymmetric catalysis in direct nitromethane-free Henry reactions. *RSC Adv.* **2020**, *10*, 2313−2326.
(23) Abazari, R.; Sanati, S.; Morsali, A.; Kirillov, A. M.; Slawin, A. M. Z.; Carpenter-Warren, C. L. Simultaneous Presence of Open Metal Sites and Amine Groups on a 3D Dy(III)-Metal−Organic Framework Catalyst for Mild and Solvent-Free Conversion of CO2 to Cyclic Carbonates. *Inorg. Chem.* **2021**, *60*, 2056−2067.
(24) Liu, K.-G.; Sharifzadeh, Z.; Rouhani, F.; Ghorbanloo, M.; Morsali, A. Metal-organic framework composites as green/sustainable catalysts. *Coord. Chem. Rev.* **2021**, *436*, 213827.
(25) Yuan, S.; Zou, L.; Li, H.; Chen, Y.-P.; Qin, J.; Zhang, Q.; Lu, W.; Hall, M. B.; Zhou, H.-C. Flexible Zirconium Metal−Organic Frameworks as Bioinspired Switchable Catalysts. *Angew. Chem., Int. Ed.* **2016**, *55*, 10776−10780.
(26) Zhou, Y.; Abazari, R.; Chen, J.; Tahir, M.; Kumar, A.; Ikreedeegh, R. R.; Rani, E.; Singh, H.; Kirillov, A. M. Bimetallic metal−organic frameworks and MOF-derived composites: Recent progress on electro- and photoelectrocatalytic applications. *Coord. Chem. Rev.* **2022**, *451*, 214264.
(27) Li, P.; Cheng, F.-F.; Xiong, W.-W.; Zhang, Q. New synthetic strategies to prepare metal-organic frameworks. *Inorg. Chem. Front.* **2018**, *5*, 2693−2708.
(28) Yang, X.; Yuan, S.; Zou, L.; Drake, H.; Zhang, Y.; Qin, J.; Alsalme, A.; Zhou, H.-C. One-Step Synthesis of Hybrid Core-Shell Metal−Organic Frameworks. *Angew. Chem., Int. Ed.* **2018**, *57*, 3927−3932.
(29) Ghasempour, H.; Wang, K.-Y.; Powell, J. A.; ZareKarizi, F.; Lv, X.-L.; Morsali, A.; Zhou, H.-C. Metal-organic frameworks based on multicarboxylate linkers. *Coord. Chem. Rev.* **2021**, *426*, 213542.
(30) Yuan, S.; Feng, L.; Wang, K.; Pang, J.; Bosch, M.; Lollar, C.; Sun, Y.; Qin, J.; Yang, X.; Zhang, P.; Wang, Q.; Zou, L.; Zhang, Y.; Zhang, L.; Fang, Y.; Li, J.; Zhou, H.-C. Stable Metal-Organic Frameworks: Design, Synthesis, and Applications. *Adv. Mater.* **2018**, *30*, 1704303.
(31) Gu, J. Z.; Cui, Y.; Liang, X. X.; Wu, J.; Lv, D.; Kirillov, A. M. Structurally Distinct Metal-Organic and H-Bonded Networks Derived from 5-(6-Carboxypyridin-3-yl)isophthalic Acid: Coordination and Template Effect of 4,4′-Bipyridine. *Cryst. Growth Des.* **2016**, *16*, 4658−4670.
(32) Fernández-Palacio, F.; Restrepo, J.; Gálvez, S.; Gómez-Sal, P.; Mosquera, M. E. G. Functionalized aminocarboxylate moieties as linkers for coordination polymers: influence of the substituents in the dimensionality of the final structure. *CrystEngComm* **2014**, *16*, 3376−3386.
(33) Zhai, Z.-W.; Yang, S.-H.; Luo, P.; Li, L.-K.; Du, C.-X.; Zang, S.-Q. Dicarboxylate-Induced Structural Diversity of Luminescent Zn(II)/Cd(II) Metal-Organic Frameworks Based on the 2,5-Bis(4-pyridyl)thiazolo[5,4-d]thiazole Ligand. *Eur. J. Inorg. Chem.* **2019**, *2019*, 2725−2734.
(34) Chen, C.; Zhang, W.; Zhang, M.; Bai, J. Solvents-Dependent Formation of Three MOFs from the Fe_3O Cluster and 3,3′,5,5′-Diphenyltetracarboxylic Acid and Their Selective CO_2 Adsorption. *Inorg. Chem.* **2019**, *58*, 13836−13842.
(35) Wang, Y.; Cao, H.; Zheng, B.; Zhou, R.; Duan, J. Solvent- and pH-Dependent Formation of Four Zinc Porous Coordination Polymers: Framework Isomerism and Gas Separation. *Cryst. Growth Des.* **2018**, *18*, 7674−7682.
(36) Sánchez-Férez, F.; Bayés, L.; Font-Bardia, M.; Pons, J. Solvent dependent formation of Cu(II) complexes based on isonicotinamide ligand. *Inorg. Chim. Acta* **2019**, *494*, 112−122.
(37) Dong, Y.-B.; Jiang, Y.-Y.; Li, J.; Ma, J.-P.; Liu, F.-L.; Tang, B.; Huang, R.-Q.; Batten, S. R. Temperature-dependent synthesis of metal-organic frameworks based on a flexible tetradentate ligand with bidirectional coordination donors. *J. Am. Chem. Soc.* **2007**, *129*, 4520−4521.

https://doi.org/10.1021/acs.inorgchem.2c01488
Inorg. Chem. 2022, 61, 12577−12590

(38) Kirillov, A. M.; Coelho, J. A. S.; Kirillova, M. V.; da Silva, M. F. C. G.; Nesterov, D. S.; Gruenwald, K. R.; Haukka, M.; Pombeiro, A. J. L. Bringing an "old" biological buffer to coordination chemistry: new 1D and 3D coordination polymers with $[Cu_4(Hbes)_4]$ cores for mild hydrocarboxylation of alkanes. *Inorg. Chem.* **2010**, *49*, 6390−6392.
(39) Gu, J.; Gao, Z.; Tang, Y. pH and Auxiliary Ligand Influence on the Structural Variations of 5(2′-Carboxylphenyl) Nicotate Coordination Polymers. *Cryst. Growth Des.* **2012**, *12*, 3312−3323.
(40) Akporiaye, D. E.; Dahl, I. M.; Karlsson, A.; Wendelbo, R. Combinatorial approach to the hydrothermal synthesis of zeolites. *Angew. Chem., Int. Ed.* **1998**, *37*, 609−611.
(41) Lu, J. Y. Crystal engineering of Cu-containing metal-organic coordination polymers under hydrothermal conditions. *Coord. Chem. Rev.* **2003**, *246*, 327−347.
(42) Yang, G.; Park, S.-J. Conventional and Microwave Hydrothermal Synthesis and Application of Functional Materials: A Review. *Materials* **2019**, *12*, 1177.
(43) Shandilya, M.; Rai, R.; Singh, J. Review: hydrothermal technology for smart materials. *Adv. Appl. Ceram.* **2016**, *115*, 354−376.
(44) Gu, J. Z.; Wen, M.; Liang, X.; Shi, Z.-F.; Kirillova, M. V.; Kirillov, A. M. Multifunctional Aromatic Carboxylic Acids as Versatile Building Blocks for Hydrothermal Design of Coordination Polymers. *Crystals* **2018**, *8*, 83.
(45) Gu, J. Z.; Cai, Y.; Liang, X. X.; Wu, J.; Shi, Z. F.; Kirillov, A. M. Bringing 5-(3,4-dicarboxylphenyl) picolinic acid to crystal engineering research: hydrothermal assembly, structural features, and photocatalytic activity of Mn, Ni, Cu, and Zn coordination polymers. *CrystEngComm* **2018**, *20*, 906−916.
(46) Zhao, S. Q.; Gu, J. Z. Synthesis, Structure and Catalytic Properties of Mn(II) Coordination Polymer through in Situ Ligand Reaction. *Chin. J. Inorg. Chem.* **2021**, *37*, 751−757.
(47) Furukawa, H.; Gándara, F.; Zhang, Y.-B.; Jiang, J.; Queen, W. L.; Hudson, M. R.; Yaghi, O. M. Water Adsorption in Porous Metal-Organic Frameworks and Related Materials. *J. Am. Chem. Soc.* **2014**, *136*, 4369−4381.
(48) Peng, S.; Bie, B.; Jia, H.; Tang, H.; Zhang, X.; Sun, Y.; Wei, Q.; Wu, F.; Yuan, Y.; Deng, H.; Zhou, X. Efficient Separation of Nucleic Acids with Different Secondary Structures by Metal-Organic Frameworks. *J. Am. Chem. Soc.* **2020**, *142*, 5049−5059.
(49) Zheng, J.; Barpaga, D.; Trump, B. A.; Shetty, M.; Fan, Y.; Bhattacharya, P.; Jenks, J. J.; Su, C.-Y.; Brown, C. M.; Maurin, G.; McGrail, B. P.; Motkuri, R. K. Molecular Insight into Fluorocarbon Adsorption in Pore Expanded Metal-Organic Framework Analogs. *J. Am. Chem. Soc.* **2020**, *142*, 3002−3012.
(50) Maserati, L.; Meckler, S. M.; Li, C.; Helms, B. A. Minute-MOFs: Ultrafast Synthesis of M-2(dobpdc) Metal-Organic Frameworks from Divalent Metal Oxide Colloidal Nanocrystals. *Chem. Mater.* **2016**, *28*, 1581−1588.
(51) Siegelman, R. L.; Milner, P. J.; Forse, A. C.; Lee, J.-H.; Colwell, K. A.; Neaton, J. B.; Reimer, J. A.; Weston, S. C.; Long, J. R. Water Enables Efficient CO_2 Capture from Natural Gas Flue Emissions in an Oxidation-Resistant Diamine-Appended Metal-Organic Framework. *J. Am. Chem. Soc.* **2019**, *141*, 13171−13186.
(52) Groom, C. R.; Bruno, I. J.; Lightfoot, M. P.; Ward, S. C. The Cambridge Structural Database. *Acta Crystallogr., Sect. B: Struct. Sci., Cryst. Eng. Mater.* **2016**, *72*, 171−179.
(53) Peng, S.; Bie, B.; Sun, Y.; Liu, M.; Cong, H.; Zhou, W.; Xia, Y.; Tang, H.; Deng, H.; Zhou, X. Metal-organic frameworks for precise inclusion of single-stranded DNA and transfection in immune cells. *Nat. Commun.* **2018**, *9*, 1293.
(54) Deng, H.; Grunder, S.; Cordova, K. E.; Valente, C.; Furukawa, H.; Hmadeh, M.; Gándara, F.; Whalley, A. C.; Liu, Z.; Asahina, S.; Kazumori, H.; O'Keeffe, M.; Terasaki, O.; Stoddart, J. F.; Yaghi, O. M. Large-Pore Apertures in a Series of Metal-Organic Frameworks. *Science* **2012**, *336*, 1018−1023.
(55) Liu, X.; Wang, X.; Gao, T.; Xu, Y.; Shen, X.; Zhu, D. Three 3D lanthanide-organic frameworks with sra topology: syntheses, structures, luminescence and magnetic properties. *CrystEngComm* **2014**, *16*, 2779−2787.
(56) Milner, P. J.; Martell, J. D.; Siegelman, R. L.; Gygi, D.; Weston, S. C.; Long, J. R. Overcoming double-step CO_2 adsorption and minimizing water co-adsorption in bulky diamine-appended variants of Mg_2(dobpdc). *Chem. Sci.* **2018**, *9*, 160−174.
(57) Kim, H.; Lee, H. Y.; Kang, D. W.; Kang, M.; Choe, J. H.; Lee, W. R.; Hong, C. S. Control of the Metal Composition in Bimetallic Mg/Zn(dobpdc) Constructed from a One-Dimensional Zn-Based Template. *Inorg. Chem.* **2019**, *58*, 14107−14111.
(58) Runcevski, T.; Xu, J.; Srebro-Hooper, M.; Milner, P. J.; Colwell, K. A.; Autschbach, J.; Reimer, J. A.; Long, J. R. Enantioselective Recognition of Ammonium Carbamates in a Chiral Metal−Organic Framework. *J. Am. Chem. Soc.* **2017**, *139*, 16000−16012.
(59) Forse, A. C.; Gonzalez, M. I.; Siegelman, R. L.; Witherspoon, V. J.; Jawahery, S.; Mercado, R.; Milner, P. J.; Martell, J. D.; Smit, B.; Blümich, B.; Long, J. R.; Reimer, J. A. Unexpected Diffusion Anisotropy of Carbon Dioxide in the Metal-Organic Framework Zn_2(dobpdc). *J. Am. Chem. Soc.* **2018**, *140*, 1663−1673.
(60) Siegelman, R. L.; McDonald, T. M.; Gonzalez, M. I.; Martell, J. D.; Milner, P. J.; Mason, J. A.; Berger, A. H.; Bhown, A. S.; Long, J. R. Controlling Cooperative CO2 Adsorption in Diamine-Appended Mg_2(dobpdc) Metal-Organic Frameworks. *J. Am. Chem. Soc.* **2017**, *139*, 10526−10538.
(61) McGuirk, C. M.; Siegelman, R. L.; Drisdell, W. S.; Runčevski, T.; Milner, P. J.; Oktawiec, J.; Wan, L. F.; Su, G. M.; Jiang, H. Z. H.; Reed, D. A.; Gonzalez, M. I.; Prendergast, D.; Long, J. R. Cooperative adsorption of carbon disulfide in diamine-appended metal-organic frameworks. *Nat. Commun.* **2018**, *9*, 5133.
(62) McDonald, T. M.; Lee, W. R.; Mason, J. A.; Wiers, B. M.; Hong, C. S.; Long, J. R. Capture of Carbon Dioxide from Air and Flue Gas in the Alkylamine-Appended Metal-Organic Framework mmen-Mg_2(dobpdc). *J. Am. Chem. Soc.* **2012**, *134*, 7056−7065.
(63) McDonald, T. M.; Mason, J. A.; Kong, X.; Bloch, E. D.; Gygi, D.; Dani, A.; Crocellà, V.; Giordanino, F.; Odoh, S. O.; Drisdell, W. S.; Vlaisavljevich, B.; Dzubak, A. L.; Poloni, R.; Schnell, S. K.; Planas, N.; Lee, K.; Pascal, T.; Wan, L. F.; Prendergast, D.; Neaton, J. B.; Smit, B.; Kortright, J. B.; Gagliardi, L.; Bordiga, S.; Reimer, J. A.; Long, J. R. Cooperative insertion of CO_2 in diamine-appended metal-organic frameworks. *Nature* **2015**, *519*, 303−308.
(64) Gygi, D.; Bloch, E. D.; Mason, J. A.; Hudson, M. R.; Gonzalez, M. I.; Siegelman, R. L.; Darwish, T. A.; Queen, W. L.; Brown, C. M.; Long, J. R. Hydrogen Storage in the Expanded Pore Metal-Organic Frameworks M-2(dobpdc) (M = Mg, Mn, Fe, Co, Ni, Zn). *Chem. Mater.* **2016**, *28*, 1128−1138.
(65) Sheldrick, G. M. Phase annealing in SHELX-90: direct methods for larger structures. *Acta Crystallogr., Sect. A: Found. Crystallogr.* **1990**, *46*, 467−473.
(66) Sheldrick, G. M. *SHELXS-97, A Program for X-ray Crystal Structure Solution, and SHELXL-97, A Program for X-ray Structure Refinement*; Göttingen University: Germany, 1997.
(67) Spek, A. L. PLATON SQUEEZE: a tool for the calculation of the disordered solvent contribution to the calculated structure factors. *Acta Crystallogr., Sect. C: Struct. Chem.* **2015**, *71*, 9−18.
(68) Blatov, V. A. *Multipurpose crystallochemical analysis with the program package topos*; IUCr CompComm Newslett, 2006; Vol. 7, p 4.
(69) Blatov, V. A.; Shevchenko, A. P.; Proserpio, D. M. Applied Topological Analysis of Crystal Structures with the Program Package ToposPro. *Cryst. Growth Des.* **2014**, *14*, 3576−3586.
(70) Zhou, X.; Guo, X.; Liu, L.; Shi, Z.; Pang, Y.; Tai, X. Synthesis, Crystal Structures, and Magnetic Properties of Three Cobalt(II) Coordination Polymers Constructed from 3,5-Pyridinedicarboxylic Acid or 3,4-Pyridinedicarboxylic Acid Ligands. *Crystals* **2019**, *9*, 166.
(71) Gu, J. Z.; Liang, X. X.; Cui, Y. H.; Wu, J.; Shi, Z. F.; Kirillov, A. M. Introducing 2-(2-carboxyphenoxy)terephthalic acid as a new versatile building block for design of diverse coordination polymers: synthesis, structural features, luminescence sensing, and magnetism. *CrystEngComm* **2017**, *19*, 2570−2588.

https://doi.org/10.1021/acs.inorgchem.2c01488
Inorg. Chem. 2022, 61, 12577−12590

(72) Nasani, R.; Saha, M.; Mobin, S. M.; Martins, L. M. D. R. S.; Pombeiro, A. J. L.; Kirillov, A. M.; Mukhopadhyay, S. Copper-organic frameworks assembled from in situ generated 5-(4-pyridyl)tetrazole building blocks: synthesis, structural features, topological analysis and catalytic oxidation of alcohols. *Dalton Trans.* **2014**, *43*, 9944−9954.
(73) Kirillova, M. V.; Kirillov, A. M.; Martins, A. N. C.; Graiff, C.; Tiripicchio, A.; Pombeiro, A. J. L. Topologically Unique Heterometallic Cu-II/Li Coordination Polymers Self-Assembled from N,N-bis(2-Hydroxyethyl)-2-aminoethanesulfonic Acid Biobuffer: Versatile Catalyst Precursors for Mild Hydrocarboxylation of Alkanes to Carboxylic Acids. *Inorg. Chem.* **2012**, *51*, 5224−5234.
(74) Gu, J.-Z.; Wan, S.-M.; Dou, W.; Kirillova, M. V.; Kirillov, A. M. Coordination polymers from an unexplored biphenyl-tricarboxylate linker: hydrothermal synthesis, structural traits and catalytic cyanosilylation. *Inorg. Chem. Front.* **2021**, *8*, 1229−1242.
(75) Gu, J.; Wan, S.; Cheng, X.; Kirillova, M. V.; Kirillov, A. M. Coordination Polymers from 2-Chloroterephthalate Linkers: Synthesis, Structural Diversity, and Catalytic CO_2 Fixation. *Cryst. Growth Des.* **2021**, *21*, 2876−2888.
(76) Zhao, S. Q.; Gu, J. Z. Syntheses, Structures and Catalytic Properties of Two Mn(II) and Cd(II) Coordination Polymers through in Situ Ligand Reaction. *Chin. J. Struct. Chem.* **2021**, *40*, 785−796.
(77) Li, N.; Feng, R.; Zhu, J.; Chang, Z.; Bu, X.-H. Conformation versatility of ligands in coordination polymers: From structural diversity to properties and applications. *Coord. Chem. Rev.* **2018**, *375*, 558−586.
(78) Gu, J. Z.; Cai, Y.; Wen, M.; Shi, Z. F.; Kirillov, A. M. A new series of Cd(II) metal-organic architectures driven by soft ether-bridged tricarboxylate spacers: synthesis, structural and topological versatility, and photocatalytic properties. *Dalton Trans.* **2018**, *47*, 14327−14339.
(79) Gu, J.-Z.; Liang, X.-X.; Cai, Y.; Wu, J.; Shi, Z.-F.; Kirillov, A. M. Hydrothermal assembly, structures, topologies, luminescence, and magnetism of a novel series of coordination polymers driven by a trifunctional nicotinic acid building block. *Dalton Trans.* **2017**, *46*, 10908−10925.
(80) Ballini, R.; Palmieri, A. *Nitroalkanes: Synthesis, Reactivity, and Applications*; John Wiley & Sons, 2021.
(81) Loukopoulos, E.; Kostakis, G. E. Review: Recent advances of one-dimensional coordination polymers as catalysts. *J. Coord. Chem.* **2018**, *71*, 371−410.
(82) Gupta, A. K.; De, D.; Bharadwaj, P. K. A NbO type Cu(II) metal-organic framework showing efficient catalytic activity in the Friedlander and Henry reactions. *Dalton Trans.* **2017**, *46*, 7782−7790.
(83) Karmakar, A.; Martins, L. M. D. R. S.; Hazra, S.; Guedes da Silva, M. F. C.; Pombeiro, A. J. L. Metal-Organic Frameworks with Pyridyl-Based Isophthalic Acid and Their Catalytic Applications in Microwave Assisted Peroxidative Oxidation of Alcohols and Henry Reaction. *Cryst. Growth Des.* **2016**, *16*, 1837−1849.
(84) Pal, S.; Maiti, S.; Nayek, H. P. A three-dimensional (3D) manganese (II) coordination polymer: Synthesis, structure and catalytic activities. *Appl. Organomet. Chem.* **2018**, *32*, 4447.
(85) Karmakar, A.; Guedes da Silva, M. F. C.; Hazra, S.; Pombeiro, A. J. L. Zinc amidoisophthalate complexes and their catalytic application in the diastereoselective Henry reaction. *New J. Chem.* **2015**, *39*, 3004−3014.
(86) Karmakar, A.; Rúbio, M. D. M.; Guedes da Silva, M. F. C.; Pombeiro, A. J. L. Synthesis of metallomacrocycle and coordination polymers with pyridine-based amidocarboxylate ligands and their catalytic activity towards the Henry and Knoevenagel reactions. *ChemistryOpen* **2018**, *7*, 865−877.
(87) Pal, S.; Maiti, S.; Nayek, H. P. A three-dimensional (3D) manganese (II) coordination polymer: Synthesis, structure and catalytic acitivities. *Appl. Organomet. Chem.* **2018**, *32*, No. e4447.
(88) Hazra, S.; Karmakar, A.; Guedes da Silva, M. F. C.; Dlháň, L.; Boča, R.; Pombeiro, A. J. L. Sulfonated Schiff base dinuclear and polymetric copper(II) complexes: crystal structures, magnetic properties and catalytic application in Henry reaction. *New J. Chem.* **2015**, *39*, 3424−3434.
(89) Kopylovich, M. N.; Mac Leod, T. C. O.; Mahmudov, K. T.; Guedes da Silva, M. F. C.; Pombeiro, A. J. L. Zinc(II) *ortho*-hydroxyphenylhydrazo-*β*-diketonate complexes and their catalytic ability towards diastereoselective nitroaldol (Henry) reaction. *Dalton Trans.* **2011**, *40*, 5352−5361.
(90) Gupta, M.; Vittal, J. J. Control of interpenetration and structural transformations in the interpenetrated MOFs. *Coord. Chem. Rev.* **2021**, *435*, 213789.
(91) Jiang, H.-L.; Makal, T. A.; Zhou, H.-C. Interpenetration control in metal-organic frameworks for functional applications. *Coord. Chem. Rev.* **2013**, *257*, 2232−2249.

https://doi.org/10.1021/acs.inorgchem.2c01488
Inorg. Chem. 2022, 61, 12577−12590